Delft University of Technology

Additional thesis

The impact of spatial sampling and signal-to-noise ratio on image quality in onshore seismics

Adriaan VISSER 4202724

Start date: 1st September 2017
End date: 18th December 2017

Supervisors:
Prof. Dr. Ir. R. F. Hanssen
P. Dheenathayalan, MSc

This additional thesis is written as partial fulfilment for obtaining the degree of
Master of Science in Applied Earth Sciences
Course: AES4011-10
Credits: 10 ECTS

Abstract

An onshore seismic survey is best conducted symmetrically, due to the reciprocity theorem of the wave field. Within the family of symmetric geometries the cross spread is most used. Recent developments show a marked increase of the number of available channels, nowadays 100,000+. This enables the use of point receivers, meaning that every geophone has its output recorded, instead of being in an array which is summed before sending the data.

Geophones are ever increasing in capability, seeing an increase to lower corner frequencies and the use of batteries and GPS systems to make them cableless and suitable for point-receiver recording. MEMS are new on the market, with a noise floor of < 15 ng/$\sqrt{\text{Hz}}$ being available. The two main quantities which are not specified in the manufacturers' data sheets of geophones, but which are highly relevant to the user are the noise floor and the dynamic operating range.

The case study shows that most surveys nowadays are 3D cross-spread surveys with a source and receiver spacing of approximately 40m each.

The most used data format in the geophysical industry is SEG-Y.

A synthetic subsurface model has been generated, through which shots have been modelled. Using real field data from Saudi Aramco tests have been conducted to both increase the shot and receiver interval, and to add various amounts of noise to this data. The shots have subsequently been migrated to generate a subsurface image, for which two methods of quality control have been devised: the correlation of the image with respect to the full, no-noise model, and the number of lines as detected through the Canny edge method. The quantity spatial interval over SNR has been used to create a function for both QC methods; $Corr = 117.862/(\frac{SI}{SNR} + 114.650)$, and $N_l \propto (SI/SNR)^{1/4}$ for the number of lines. The fit for the number of lines has a very low R^2, hence a new method must be sought for quality control.

For the given model $SI/SNR = 75$ has been selected as a maximum for this ratio to obtain a migrated result of sufficient quality for it to be able to be interpreted.

Contents

1 Introduction

Seismic acquisition on land has undergone quite a few technological advances over the past decades. Everything is aimed at getting the highest quality image with the lowest amount of money spent. Industry has shifted from a few 2D receiver lines to large 4D acquisition systems with hundreds of thousands of channels. Changing acquisition geometries and an increase of available channels lead to a change from receiver arrays to point receivers. In order to get at least the same, but preferably a better signal-to-noise ratio (SNR), it is important to know what the influence of noise is on the quality of the final migrated result.

Therefor it is important to know to what extend the noise influences the signal, and how far the source and receiver positions can be spread apart to still get meaningful data about the subsurface. In order to answer this question the following sub-questions will be answered:

- What is the spatial sampling and SNR currently in use to give industry quality data?

- What is the impact of reduced spatial sampling and SNR on data quality?

- What are the data formats being used in the industry?

This report first gives an overview of the current state of seismic acquisition on land, section 2, then discusses geophones, section 3, presents an overview of recent case studies, section 4, and concludes with a short remark on the current data formats which are used in the seismic industry, section 5. Then an example of how spatial sampling and SNR influence the quality of a seismic image is given on basis of a synthetic model, section 6. Finally recommendations for future research are given, section 7.

2 Seismic surveys: requirements and design

This section outlines the basic requirements of onshore acquisition geometry and design requirements, sections 2.1, 2.2 and 2.3, as presented by Vermeer, 2002. Finally recent developments with regard to the increase of available channels and single sensor technology are given, section 2.4.

2.1 Objective of a survey

A seismic survey is conducted with a few objectives in mind, see Vermeer 2002, section 4.2:

- Structural interpretation

- Stratigraphic interpretation

- Reservoir characterisation

  - Porosity
  - Pore fill
  - Fracture orientation

- Time lapse

The structural interpretation is desired in order to know the geometry of the subsurface, such as faults, anticlines, pinch-outs, etc., which can function as an oil trap. Stratigraphic information is obtained from the estimated velocity and density of a geological layer, in order to find reservoir rocks. Once a trapped reservoir rock has been found, parameters of the reservoir, such as porosity and pore infill, need to be characterised. The time lapse, finally, is used in reservoir monitoring during production, e.g. to check on the progress of steam injection.

2.2 Choice of geometry

The first consideration to be made with respect to geometry is symmetry. The reciprocity theorem states that the wave field is identical when the location of source and receiver are interchanged (Fokkema and Van den Berg 1993). As a consequence the wave field in a common-shot gather shot at point $W(t, x_p, x_r)$ is equal to the wave field of the common-receiver gather $W(t, x_s, x_p)$, recorded at the same point, i.e. $x_s = x_r = x_p$. Since shots and receivers are virtually the same in terms of spatial antialiasing, this leads to the conclusion that a symmetric sampling of shots and receivers is preferred. Additionally, for migrational purposes it is practical to have a symmetric sampling of both receivers and shots, as virtual shots and receivers are modelled in the subsurface on the same point, easing the computations.

The geometry of the survey should act as a spatial antialias filter, i.e. $\Delta x_s = \Delta x_r \leq \frac{1}{2k_{max}} = \frac{V_{min}}{2f_{max}}$; where k_{max} is the maximum wave number, which is determined by the maximum frequency f_{max} present in the data. V_{min} is the velocity of the slowest event which needs to be modelled. For a ground roll of 300 m/s, recorded with maximum frequency 75 Hz the shot and receiver interval should be ≤ 2 m, which is far too expensive in practise.

2.2.1 Cross spread

The most used geometry for onshore acquisition is the cross spread (fig. 1). The cross spread is easy to lay out, is easily adapted to go around physical obstacles, and has a high fold across the whole domain, where fold is the number of common midpoints located in a given bin, which are summed to result in a single stacked trace. The source and receiver lines are laid out perpendicular to one another, resulting in a full azimuth coverage. When repeating the template many times, thus using many source and receiver lines, a high fold is easily obtained for the whole data set, making it ideal for dual-domain filtering.
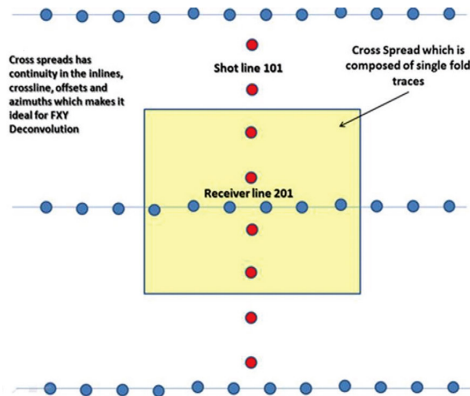

Figure 1: Template of a cross-spread for seismic survey. The blue dots are receiver stations, the red dots shot stations. Image taken from Schulte and Manthei, 2014.

2.2.2 Other symmetric geometries

The parallel geometry (fig. 3) has the receiver lines and shot lines in parallel. This results in high inline fold, but a low crossline fold, even as low as 1 for a single parallel receiver/shot line pair. The benefits of doing a parallel acquisition are a better stack response for linear noise suppression than in the cross spread case, and much easier processing of the data (Vermeer, 1998). The main drawback of parallel acquisition is that unlimited access is required to the area, which is practically impossible except for deserted areas without obstructions such as a desert or tundra. The density of lines results

in a high cost, and since the data is almost single azimuth, this geometry is not well suited for difficult geology in which illumination from all sides is necessary.

For open areas such as deserts the zigzag geometry is the most efficient in terms of acquisition time, since the travel distance of the vibrators is a factor $\sqrt{2}$ less than in the orthogonal case. This geometry also has less crossings of shot- and receiver lines, meaning a lower chance of trucks running over the geophones. The zigzag has limited azimuth variation, slightly more than the parallel case, but a lot less compared to the cross spread. This means a smoother multiple moveout in processing. Depending on whether the shots or receivers are zigzagged, the shots or receivers are oversampled with a factor of $\sqrt{2}$ in the in-line direction, and migration is more likely to alias. Ground roll suppression is usually done by dual-domain filtering, (f, k) frequency, wave number, which cannot be carried out in this geometry due to the variable length of common-receiver gathers. Additionally amplitudes of the signal are more difficult to control due to the lower apparent velocity of the signal. Finally this geometry requires longer shot lines than in the orthogonal case, increasing the cost of the survey, especially in difficult terrain.
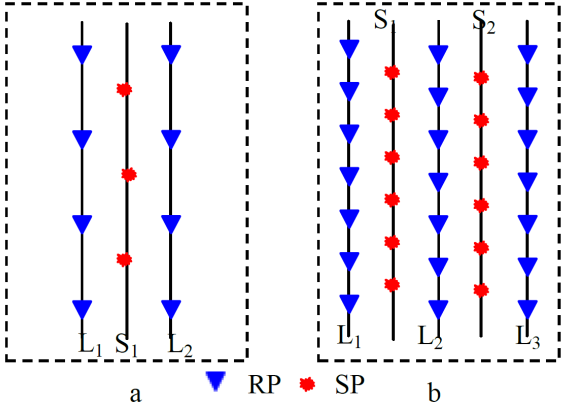

Figure 2: Template of a parallel geometry for seismic survey. The blue dots are receiver stations, the red dots shot stations. *Schematics of the conventional and the high density wide line (a: the conventional wide line; b: the high density wide line; L: receiver line; S: source line)* Image taken from Wu et al., 2017.
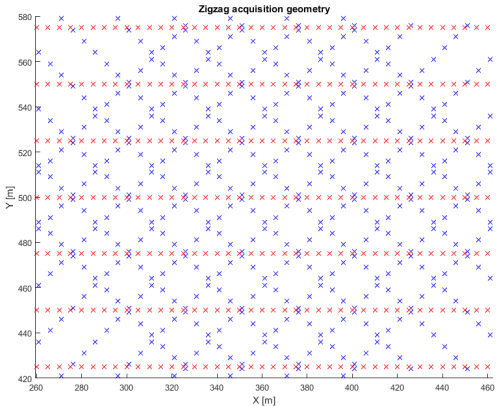

Figure 3: Template of a zigzag geometry for seismic survey. The blue crosses are receiver stations, the red crosses shot stations, or vice-versa.

2.3 Design of a survey

On basis of the above considerations a design sketch for a symmetric, orthogonal survey will be presented, based on section 4.4 of Vermeer, 2002.

- Set the shot and receiver interval, $\Delta s = \Delta r$

- Determine the depth, in metre or travel distance, of the shallowest horizon of interest; set a requirement on the fold coverage, M, for that horizon.

- Find the maximum offset of the shallowest horizon x_{sh}.

- Calculate the line interval $S \approx \frac{x_{sh}}{\sqrt{2M}}$, and choose S as the nearest integer multiple of the shot interval ΔS.

- Determine the depth of the deepest horizon to be mapped.

- Find the maximum offset x_{dp} for that horizon.

- Calculate the spread length $L = 2x_{dp}$, and choose the L as the nearest integer multiple of S

- Find inline, crossline and total fold M_i, M_x and M; $M_i = M_x = \sqrt{M}$ in the symmetric case.

- Find number of receiver lines N_R and number of channels per line N_{chl}; The total number of active channels $N_{tot} = N_R N_{chl}$.

- Calculate the shot density per square kilometre $S_{dens} = 10^6/(\Delta s S)$.

- Find the distance to build full fold coverage $D = (X_{max} - S)/2$.

As an example table 4.4 from Vermeer 2002 is reproduced here (table 1).

Table 1: Formulas for survey parameters (equal line spacings). Copied from Vermeer, 2002, table 4.4

Parameter	Formula	Example
Station spacings	$\Delta s, \Delta r$	25 m
Maximum inline and crossline offset	X_{max}	3500 m
Line interval	S	700 m
Bin size	$b = \Delta s \Delta r / 4$	$b = 12.5 \times 12.5$ m
Spread length	$L = 2X_{max}$	$L = 7000$ m
Inline fold	$M_i = L/2S$	$M_i = 7000/1400 = 5$
Crossline fold	$M_x = M_i$	$M_x = 5$
Total fold	$M = M_i M_x$	$M = 25$
Number of receiver lines	$N_R = 2M_x$	$N_R = 10$
Number of channels per line	$N_{chl} = 2X_{max}/\Delta r$	$N_{chl} = 280$
Total number of active channels	$N_{tot} = N_{chl} N_R$	$N_{tot} = 2800$
Number of shots / km^2	$S_{dens} = 1\,000\,000/(\Delta s S)$	$S_{dens} = 57.1/\text{km}^2$
Distance to build full fold	$D = (X_{max} - S)/2$	$D = 1400$ m

2.4 Recent developments

Recent innovations show a trend to use more and more channels, some systems having 100,000+. This has a huge impact on acquisition geometries, as the necessity to have a symmetric geometry decreases with increasing number of channels. Symmetric acquisition, as advocated by Vermeer, 2002, is employed mainly to act as a spatial anti-alias and spatial noise filter. However, according to Dean,

2012, digital noise filtering is vastly superior, having the capability of using 10-20% of the sensors of a traditional survey, whilst having comparable image quality. The main reason for this is that in traditional field arrays a certain amount of geophones is placed in a spatial geometry such as to act as a spatial antialias filter, and their response is stacked before storing the result.

Approximately 90% of the energy of an active shot goes into surface waves, therefor field arrays are used as spatial antialias filters (Campman et al. 2016). The basic receiver sampling interval is based on the highest expected wave number in the data, usually associated to these surface waves. Several geophones are thus put in a pattern, called a receiver array, to suppress those surface waves, and their response is summed, boosting the SNR by the square root of the number of sensors. The sensitivity of the array to the reflected signal is higher than that of individual geophones. The SNR is proportional to $\sqrt{\frac{A_F}{A_b}}$, where A_F is the area of the first Fresnel zone, given by $\delta_F = \sqrt{\frac{Z\lambda}{2}}$, where Z is the depth and λ the wavelength under consideration; and A_b is the bin size. Thus the SNR can be boosted by either decreasing line spacing, and thus increasing fold, or by decreasing the group interval, yielding smaller bins.

Using field arrays results in the data of each single geophone being irrecoverable, only the data of the combined field array is known. The location of each geophone is planned by the survey planner, but the crew placing the geophones usually did not have an accurate GPS device with them to exactly position the geophones. Instead, they were placed approximately on the location intended by the planner, but varying a small amount. This means that coherent noise gets smeared out a bit over the signal, thus decreasing the denoising effect of the array stack. Nowadays, however, the crews carry a high accuracy GPS device, so they can measure the exact location of each geophone. When each geophone is recorded individually, the noise can be stacked out much better due to the exact known location.

3   Geophones

Historically a geophone has been an analog device for measuring ground movement. A geophone consists of a spring-mounted mass which moves with respect to a stationary coil, see figure 4, left. When this mass moves through the coil a current is generated proportional to the velocity of the mass with respect to the coil. The frequency response of a spring-mounted mass is that of a harmonic oscillator, with a natural frequency around 10Hz for a typical geophone. A damping, usually of around 70%, is used to prevent resonance at the natural frequency.

Below the natural frequency the response of a geophone drops of drastically. Measuring lower frequency signals therefor requires a geophone with a lower natural frequency. However, the natural frequency is proportional to the inverse square root of the moving mass, thus a lower frequency requires an increasingly high mass. In order to be able to measure lower frequency signals without making the geophone impractically heavy microelectromechanical systems (MEMS) can be deployed. A MEMS acts as an accelerometer below its natural frequency, which is typically around 1 kHz. The signal which can be measured is small compared to that of an analog geophone, meaning that acceleration up to very low frequencies can be discerned.

Geophones are characterised by a few parameters which are listed on the specification sheets provided by geophone manufacturers, see table 2.

What one would like to know in addition to these specifications are the noise floor and dynamic operating range. The noise floor is the output of the sensor in the absence of any external perturbations, i.e. when then geophone is not moving and is either given as noise density in $V/\sqrt{Hz}$ (or $m/s^2/\sqrt{Hz}$), or as Power Spectral Density (PSD) V^2/Hz, or noise RMS (V, m/s or m/s^2) (Tellier and Lainé, 2017). Noise density is the preferred unit, since comparison of noise levels between sensors is mandatory to be made in noise density. The two are related through $N_{\mathrm{rms}} = \rho_n \sqrt{B}$, where N_{rms} is noise RMS, ρ_n is the noise density in $V/\sqrt{Hz}$ and B is the bandwidth of the signal in Hz. The noise floor of the latest generation of MEMS-sensors is < 15 $ng/\sqrt{Hz}$; being an improvement of approximately a factor of 3 over the previous generation.
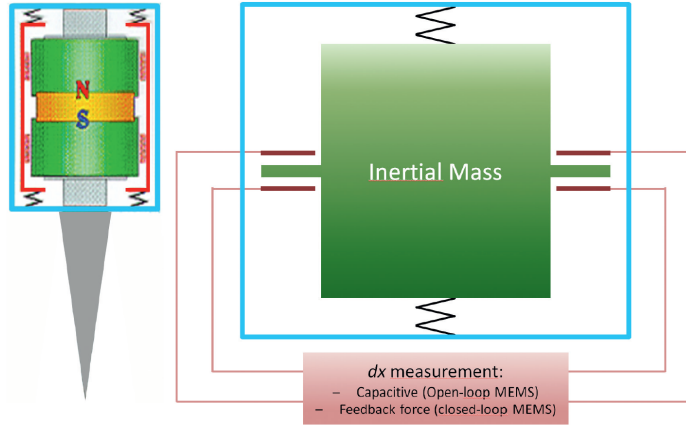
Figure 4: Geophone (left): the sensor casing (blue) is attached to a spike (grey) and to the magnet (yellow). All these components move with ground motion, while the coil (red) connected to the casing by a soft spring (black), remains motionless. Digital sensors (right): the principle is the same as for geophones on a microscopic scale, with a MEMS casing (blue) attached to a sensor casing (not represented). The inertial mass (green) is maintained by stiff springs (black) and then moves with casing/ground motions. When subjected to an acceleration, the small displacements of the inertial mass are measured by electrodes (red). Copied from Tellier and Lainé 2017, figure 1

Table 2: Typical geophone parameters as characterised on specification sheets

Parameter	Typical value
Natural frequency	4.5-10Hz
Distortion	<1%
Sensitivity	20-100V/m/s
Operating temperature	-30 to 60°C
Coil resistance	0.3-8KΩ
Tilt	15° (degrees)
Open circuit damping	0.70 (ratio)

The dynamic range is given in decibels, as $20 \cdot \log 10(\frac{V_f}{V_{rms}})$, where V_f is the maximum amplitude that can be measured, called full range, and V_{rms} is the RMS noise. Both can be in either V, m/s or m/s^2. The lower limit is equal to the Least Significant Bit (LSB) of the digitisation unit in the absence of any noise. This is considered the most important signal specification of a sensing unit, as it describes its capability to record simultaneously large and very weak signal amplitudes.

Figure 5 shows a noise density plot of a 70.7% damped 10 Hz geophone. Basically Brownian motion and electrical, Johnson, noise do not contribute much to the recorded noise, since the recording channel noise is the dominant noise source for most geophones. Campman et al., 2016, conclude that state of the art sensors and recording channels are adequate for single sensor acquisition, provided that the geometry accounts for this. Improvements in geophone=-based acquisition systems should be directed towards lowering the noise floor of the geophones.
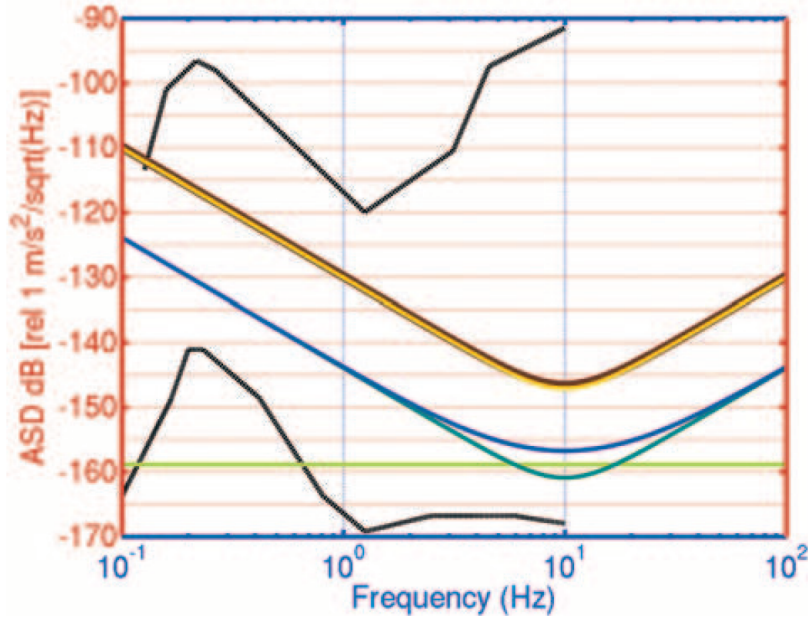
Figure 5: Example of modeled noise density contributions of a 70.7% damped, 10 Hz geophone and channel at room temperature, scaled in acceleration units. The light green line is Brownian motion noise; the dark green line is the Johnson noise; and the dark blue line is the composite noise of both. The yellow line is the referred-to-input channel noise at high gain, scaled by the sensor sensitivity. The brown line is the total geophone and channel noise. Note that the noise is dominated by the recorder, even at high gain. Copied from Campman et al. 2016, figure 2

4   Case study results

Case studies from the yearly EAGE conferences have been collected for the 77th, 78th, and 79th editions, held in 2015, 2016, and 2017. The acquisition parameters which have been used in each study are presented in table 3, where the study name refers to the code EAGE has given to that presentation, S_r is the inline receiver spacing, $S_{r,l}$ is the crossline receiver spacing, l_r is the length of the receiver line, S_s is the inline shot spacing, $S_{s,l}$ the crossline shot spacing, l_s the length of the shot lines, Area is the total acquisition area, geometry says which geometry was used for the particular surveys, and 2D/3D denotes whether the survey was conducted along a line (2D) or over an area (3D). Note that not all parameters have been filled in for each study, as not all case studies had all parameters mentioned. For these cases a dash, -, has been used to denote this. For the averages the VSP studies have been omitted, as those are very different from larger exploration or reservoir characterisation studies.

From table 3 we can conclude that for these case studies the average inline receiver spacing is almost equal to the inline shot spacing, but the crossline receiver spacing is ~1.5 times the crossline shot spacing. For the other quantities given the averages are for such a small sample size that no meaningful conclusion can be made. A possible explanation for the usage of more shots than receivers in an acquisition is that the number of possible channels is limited. Thus more receivers is not always an option due to limitations on data collection, whilst more shots just uses the existing channels more often.

Table 3: Overview of case studies of the 77th, 78th, and 79th EAGE conferences. References of the studies are given in the appendix, section 9.

Study name	S_r [m]	$S_{r,l}$ [m]	l_r [m]	S_s [m]	$S_{s,l}$ [m]	l_s[m]	Area [km^2]	Geometry	2D/3D
Th A3 09	2	-	-	5	-	-	-	VSP	2D
Th A3 12	3-7	-	-	-	-	-	-	VSP	2D
Th P6 04	24	96	-	-	-	-	18	Passive seismic	3D
Tu A2 17a	50	200	9550	50	300	2450	800	Cross-spread	3D
Tu A2 17b	25	200	11976	50	200	3200	800	Cross-spread	3D
Tu B3 08	25	-	-	50	-	-	-	Single-line	2D
We A3 07	25	250	8000	50	50	-	800	WAZ	3D
We A3 08	17	-	16000	33	-	-	-	Split-spread	3D
We B3 09a	40	280	-	40	280	-	-	Cross-spread	3D
We B3 09b	30	150	-	30	150	-	-	Cross-spread	3D
We B3 09c	150	150	-	30	30	-	-	Nodal	3D
We B3 09d	30	150	-	30	30	-	-	Carpet shooting	3D
Th SRS3 07	7.5	120	>5000	7.5	90	-	860	Point source/rec	3D
We P5 12a	25	-	-	50	-	-	-	Single line	2D
We P5 12b	50	-	-	100	-	-	-	Single line	2D
Th N114 06	50	50	-	50	50	-	-	-	-
Th P7 02	12.5/50	200	-	-	100	-	-	WAZ	3D
Th P7 06	50	250	-	50	250	-	-	Cross-spread	3D
Th P7 08	25	500	6000	25	200	6000	4500	Point source/rec	3D
Tu P3 02	50	-	-	10	-	-	180	-	-
Average	38.74	222.8	9422	40.97	144.2	3883	1137	-	-

5 Data format

The most used data format for geophone data is the SEG or SEG-Y standard, see the revised standard [5] and figure 6 (Roald van Borselen, pers comm). The first 128 bytes of the SEG-Y data format are reserved for an optional tape label. The following 3600 bytes are the Textual File Header and the Binary File Header, written as a concatenation of a 3200-byte record and a 400-byte record. After this 0 to N optional Extended Textual Headers follow. The rest of the file contains a variable number of seismic traces, each preceded by a 240-byte Standard Trace Header and 0 or more Trace Header Extensions.

Both big-endian, little-endian and pairwise byteswapped orderings are allowed; bytes 3297-3300 in the Binary File Header define which ordering the Binary File Header, Trace Headers and Trace Samples are using. The Textual Headers and Data Trailer are assumed to be text always, so they are left untouched.
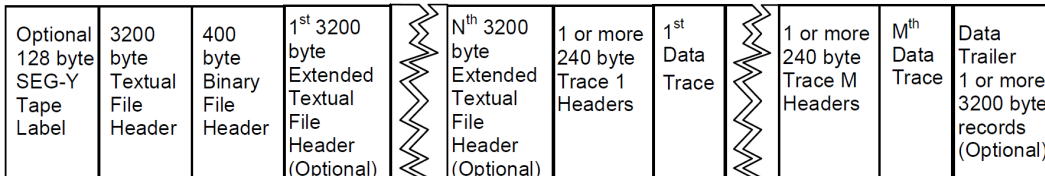

Figure 6: Byte stream structure of a SEG-Y file with N Extended Textual File Header records and M traces records. Copied from [5] figure 1.

6 Synthetic data example

In this section a synthetic data example is discussed. First the model and methodology are discussed, section 6.1, then the results are discussed, section 6.2, and finally conclusion with respect to the required spatial sampling in the presence of noise are given in section 6.3. The model and associated noise were kindly provided by Dr. Ir. D. J. Verschuur.

6.1 Model and methodology

The model is a grid of 5400 by 1250m, (x, z), using a grid size of 5×5m, containing velocity and density at each grid point. Using an acoustic finite difference modelling, second order in time, fourth order in space, staggered grid, 361 shots into 361 receivers have been modelled along the profile, with $\Delta s = \Delta r = 15$m. The model contains eight layers, from top to bottom their respective P-wave velocities in m/s are: 1750, 2000, 2300, 2600, 3500, 3150, 3400, 2900. The layer with 3500m/s is considered a "salt layer", the layer underneath that is the reservoir seal, so below that is the reservoir proper.

The noise, fig. 8, right, is from real field data from Saudi Aramco, where a random subset of shots have been stacked for each of the 361 shots so as to create a semblance of a real noise model including ground roll. The SNR is computed as $max(S)/max(N)$, where S is the signal and N the noise, both across a full common shot gather. The noise is added to the data using the **addmul** command with different weights for the noise. As an example:

```
addmul file_in1=FullModel.su file_in2=noise.su a=1 b=1 > shots_with_noise.su
```

This way the noise has been added to the model, both weighted 1, thus the SNR is 0.5. The parameter a has been kept constant at 1, and b has been varied.

Several experiments have been carried out: selecting every Nth receiver and every Mth shot, and adding noise with varying weights to this. The migrated model with all receivers and shots and no added noise is presented in figure 13, left. Spatial intervals of 15, 30, 45, 60, 75, 90, 105 and 135m have been used, as well as noise weights of 0, 1, 2, 3, 4, 5, 7, 10 and 15, where $SNR = 2/(W_n)$. A full permutation of these two parameters has been made.

The image with all sources and receivers and no noise has been considered the base image, thus all other migrated results will be quantified with respect to that one. Two test have been performed, the 2D correlation of each image with respect to the base image according to equation 1

$$r = \frac{\sum_m \sum_n (A_{mn} - \overline{A})(B_{mn} - \overline{B})}{\sqrt{(\sum_m \sum_n (A_{mn} - \overline{A})^2)(\sum_m \sum_n (B_{mn} - \overline{B})^2)}} \tag{1}$$

where A and B are the images, m, n the coordinates and $\overline{\chi}$ the mean of all pixels within the image.

A Canny edge detection [1] has been done to find lines in the image. This is expressed as the number of lines, which is the number of lines that were found using this method. The Canny edge detection results in a 1 if an edge, thus a stark contrast, has been found on that pixel and a 0 if no contrast has been found. The base image is very smooth, the only edges detected are those of actual layer boundaries. As soon as less receivers are used, or noise is introduced, more contrasts will come up and thus more, mostly short, lines will be found.

Finally a plot has been made of both the correlation coefficient and the number of lines against the quotient of spatial interval and SNR. The rationale here is that both an increase in spatial interval and a decrease in SNR have a detrimental effect on image quality and a decrease in spatial interval and increase in SNR have a positive effect on image quality. This way a ratio between the two can be found based on the requirement on the image quality.

A sample of common shot gathers using various spatial intervals and SNRs can be seen in figure 9, the associated migrated image of all shot gathers for the same given configuration is shown in figure 10.
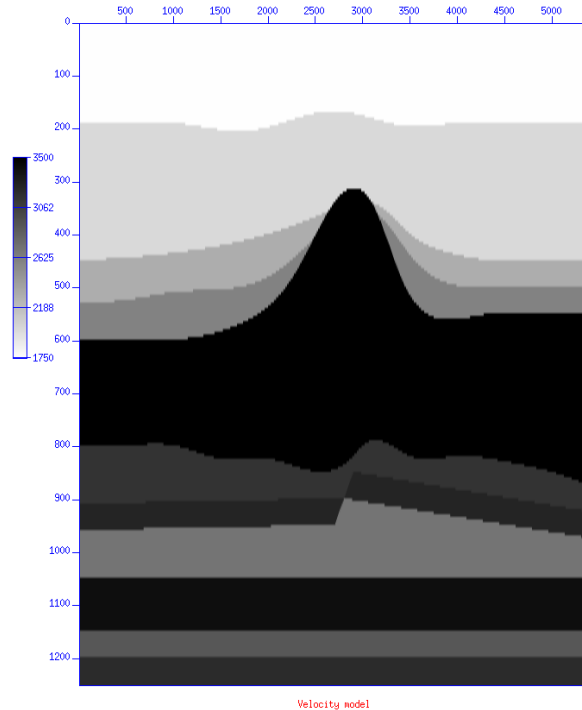
Figure 7: Synthetic subsurface velocity model.

6.2 Results

Spatial interval has quite the impact on the result, see figure 13. The left shows the migration result when using all shots and receivers, thus $\Delta s = \Delta r = 15$m, whereas on the right a subsampling has been made using every ninth shot and receiver, thus $\Delta s = \Delta r = 135$m. What is immediately obvious is that the strongly reflective layers, thus the first boundary and the top of the salt, generate migration smiles. This is not a big problem, as with the noise in the upper layers, as the layer boundaries are still clearly visible. Below the salt, however, a lot of noise emerges, making it impossible to detect any layer except the lower horizontal layer with a stark contrast. This happens because due to the coarse sampling reflection points from different receivers on a certain layer are matched to reflection points on another layer using another receiver, corrugating the imprint of shallower layers onto deeper layers.

The results of the Canny edge detection are given in figure 11. The degradation is rather marked, the left plot is clean and shows the geological boundaries, in the middle plot the upper boundaries are discernible, but distorted with lots of noise between the upper layers and the reservoir is not detected at all and the right plot shows pure noise where nothing can be verified as being an actual layer, except two stripes in the bottom right.

The result of each image compared to the base image is given in figure 15. The correlation coefficient is immediately clear: both increasing the sampling interval and decreasing the SNR result in a worse correlation of the image to the base image. This is as expected, since less data points and more noise are always detrimental to ones data. The number of lines plot is a bit less clear, apart from the general idea that a small spatial interval and low amount of noise results in a cleaner image. For the number of lines it is better to look at a few cross sections of this plot, see the second and fourth plots of figure 14. Both an increase in spatial interval an a decrease in SNR result in a higher number of lines detected. Adding noise results in approximately the same number of lines over a wide range of SNR, as is seen in the lower right of the right plot in figure 15. Without noise, a sampling interval of up to 60m has no significant detrimental effect on the image quality, as verified by the almost horizontal start of the
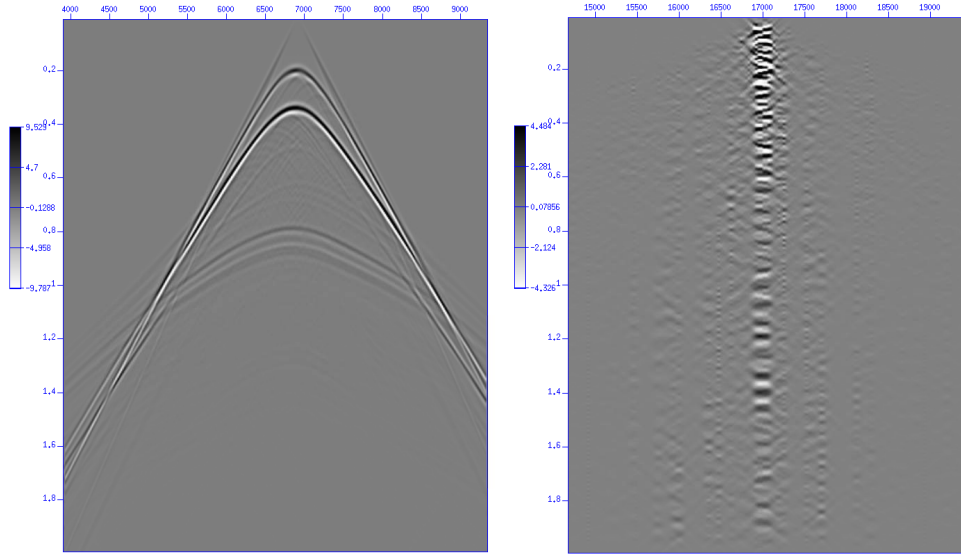
13

Figure 8: Common shot gather 200, left, with its associated noise.

blue lines in the third and fourth plots in figure 14.

As expected the image quality goes down with the increase of the quotient of spatial interval and SNR (fig. 16). The fit for the upper figure is $y = 117.862/(x + 114.650)$ with $R^2 = 0.975$, where y is the correlation coefficient and x SI/SNR, and for the lower figure $y = 57.13x^{1/4}$ with $R^2 = 0.759$, where y is the number of detected lines, and x again SI/SNR. The reason that this fit is dotted in the figure is the low value for R^2. The data suggests an asymptotic behaviour to $y = 250$, but asymptotic fits have an even lower R^2 or require many terms which are difficult to explain physically, such as $\log(\sin(x))$.

6.3   Conclusion

It can be seen that a low SNR has a detrimental effect on image quality, but since it is incoherent the layer boundaries can still be detected, even up to very low SNR. A coarse spatial interval, however, quickly gives rise to migration smiles on shallow layers and apparent ambiguities on deeper layers, especially below high velocity layers such as salt.

When noise is present the spatial interval needs to be finer than if no noise would be present. This is why seismic contractors first make a so-called noise spread in the area to find out the amount of noise they can get in their data, and base the spatial interval on that.

The fitted function for the correlation versus SI/SNR, $Correlation = 117.862/(\frac{SI}{SNR} + 114.650)$, makes sense since an increase in noise, thus a decrease in SNR, will decrease the correlation, and an increase in spatial interval, thus increasing the distance between geophones, will decrease correlation as well. The linear relationship between the distance between geophones and correlation coefficient is easy to understand, as this is a 2D case, meaning measurements on a line. Thus increasing the spatial interval will decrease the amount of receivers able to detect a reflection from a specific point in the subsurface. If this test is conducted on a 3D seismic set, thus a 2D acquisition pattern, the correlation coefficient goes down linearly with increasing the geophone distance in both x an y, thus quadratic in total.

The fit for the number of lines versus SI/SNR is rather poor, as stated before, and the choice for a fourth order root has been made on the premises that the current result is in 2D, whereas for 3D data this would be squared, thus $N_l \propto \sqrt{SI/SNR}$, which is slightly better to be explained. Again, an
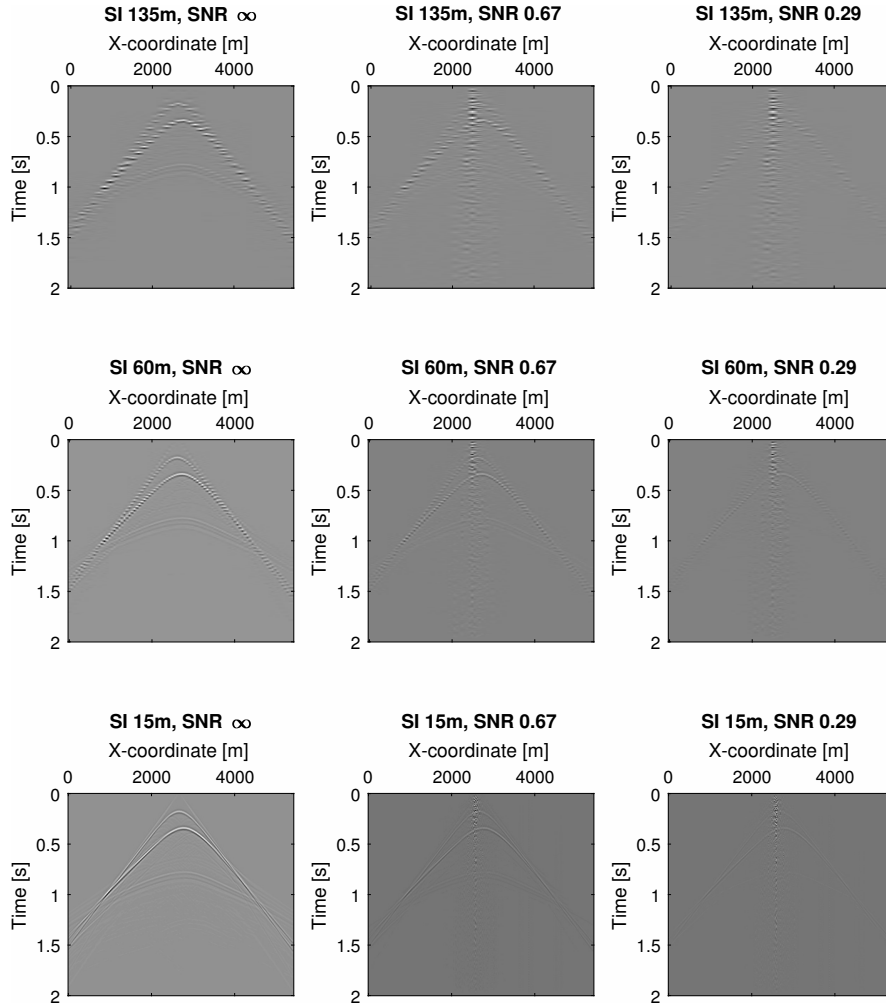
Figure 9: Middle shot gather of the data using a spatial interval of 15, 60 and 135m (bottom, middle and upper row) and SNR of ∞, 2/3 and 2/7 (left, middle and right column). Data quality clearly degrades from the lower right towards the upper left.

increase in sampling interval results, as well as an increase in noise, in more lines being detected by the Canny method. This metric is highly dependent on the geometry choices of the data acquisition, as a larger maximum depth can accommodate more geological layers, and a deeper and/or wider model can accommodate more noise, and thus more lines detected from that noise. There will be for each data set a maximum number of lines which can be present in the geometrical extend, and adding more noise or lowering the spatial sampling will not increase beyond this number, hence an asymptotic fit must be sought for this metric, or another metric must be chosen.

An $SI/SNR = 75$ has been selected as minimal requirement on the data acquisition for this specific example, as above this the image quality degrades significantly, see figure 17. This means that a minimal correlation of 0.62 and a maximal number of detected lines of 168 are required.
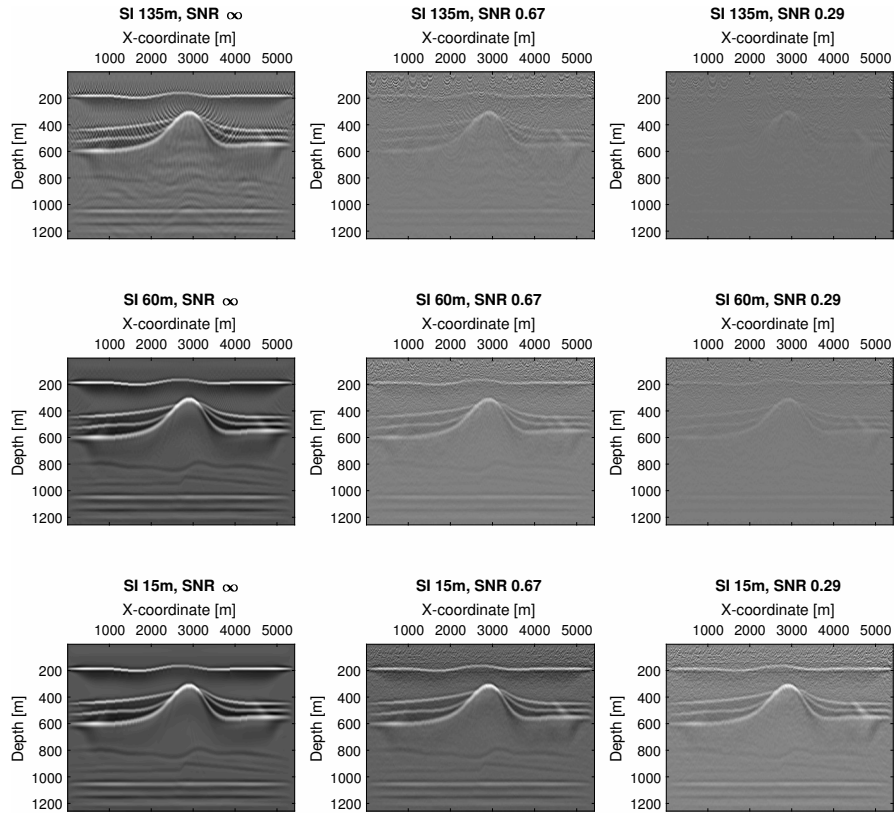
Figure 10: Migration results using a spatial interval of 15, 60 and 135m (bottom, middle and upper row) and SNR of ∞, 2/3 and 2/7 (left, middle and right column). It is clear that the lower left is the best result and image quality degrades towards the upper right.
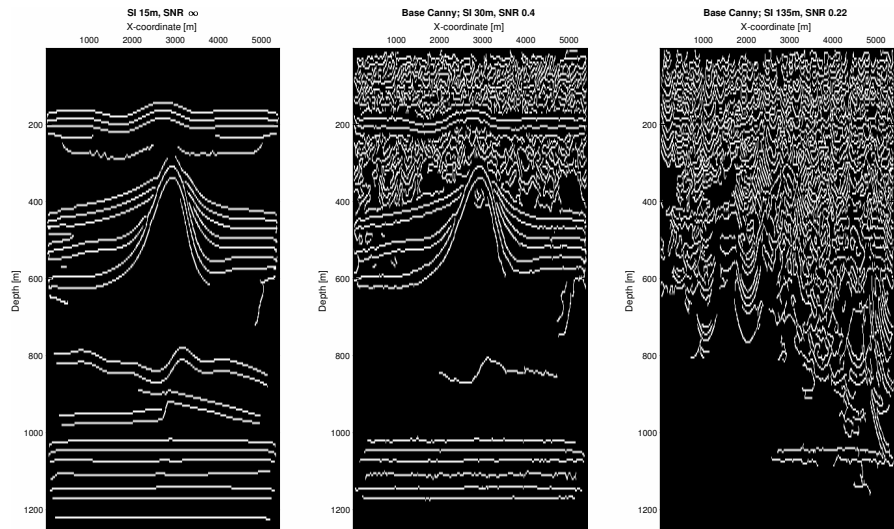

Figure 11: Results of the Canny edge detection. Every contrast detected results in a white pixel in the plot. The left plot is the base image, the middle plot has a spatial interval of 30m and SNR of 0.4, the right image a spatial interval of 135m and SNR of 0.22.

ss 15m, SNR 0.40

X-coordinate [m]

500 1000 1500 2000 2500 3000 3500 4000 4500 5000

ss 15m, SNR 0.20

X-coordinate [m]

500 1000 1500 2000 2500 3000 3500 4000 4500 5000
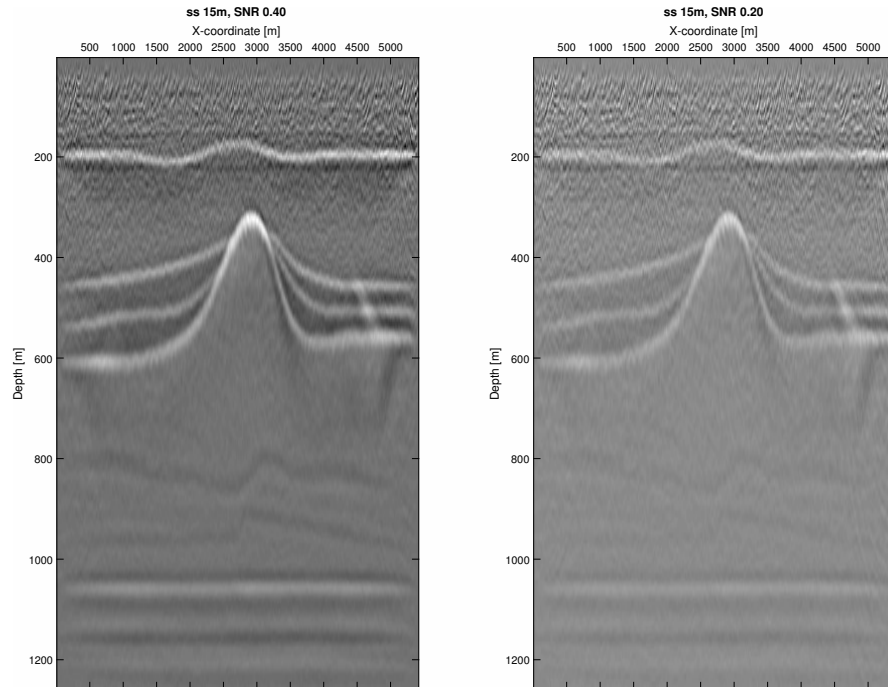
Figure 12: Migrated data using all sources and receivers, i.e. $\Delta s = \Delta r = 15$m, the figure on the left has an SNR of 0.4, the one on the right an SNR of 0.2.
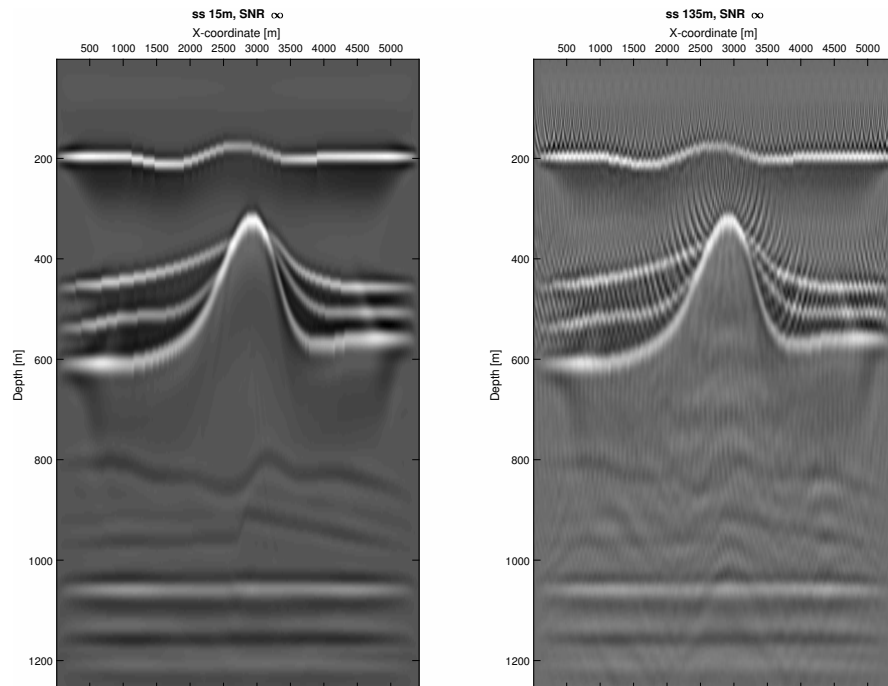
ss 15m, SNR ∞

X-coordinate [m]

500 1000 1500 2000 2500 3000 3500 4000 4500 5000

ss 135m, SNR ∞

X-coordinate [m]

500 1000 1500 2000 2500 3000 3500 4000 4500 5000

Figure 13: Left: migration using a shot and receiver spacing of 15m, right: migration using a shot and receiver spacing of 135m. Both records contain no noise. Note the prominent migration smiles in the result using $\Delta s = \Delta r = 135$m, and the inclusion of corrugation below the salt layer.
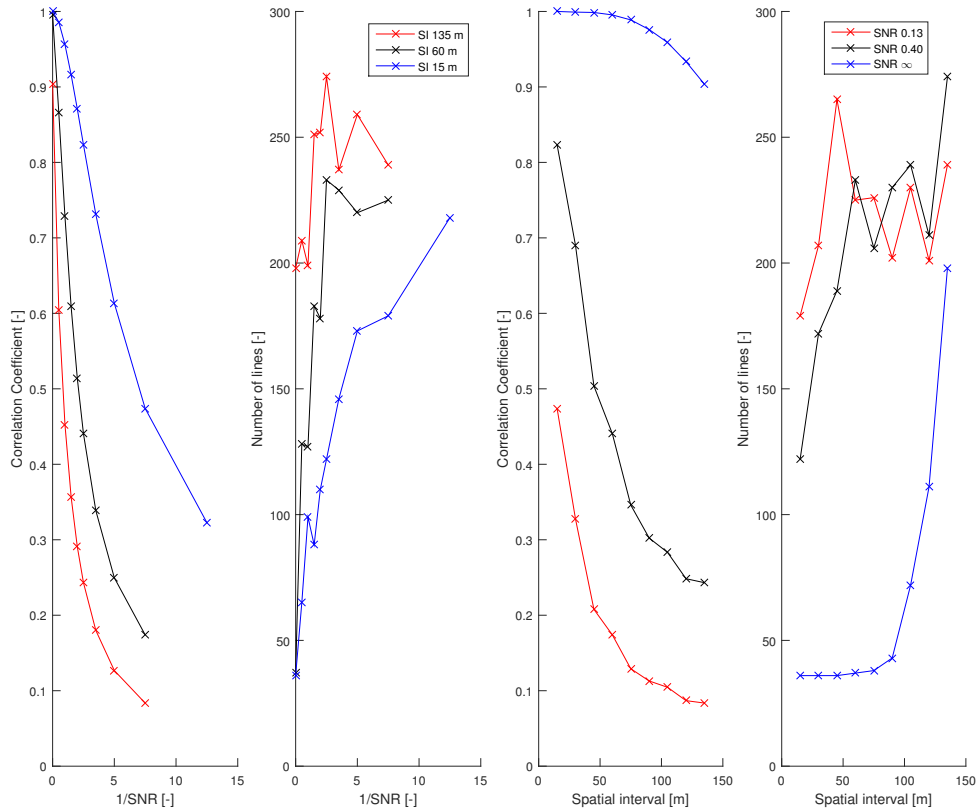
17

Figure 14: The left-most plot show the effect of SNR on the correlation with the original image, the second plot from the left shows the effect of SNR on the number of lines detected by the canny method, both plots are given for three different source/receiver intervals: 15m (blue), 60m (black) and 135m (red). The second plot from the right shows the effect of spatial interval on the correlation coefficient, the right-most plot shows the effect of spatial interval on the number of lines detected, both plots are given for three different SNRs: infinity, i.e. noise free, (blue), 0.40 (black) and 0.13 (red).
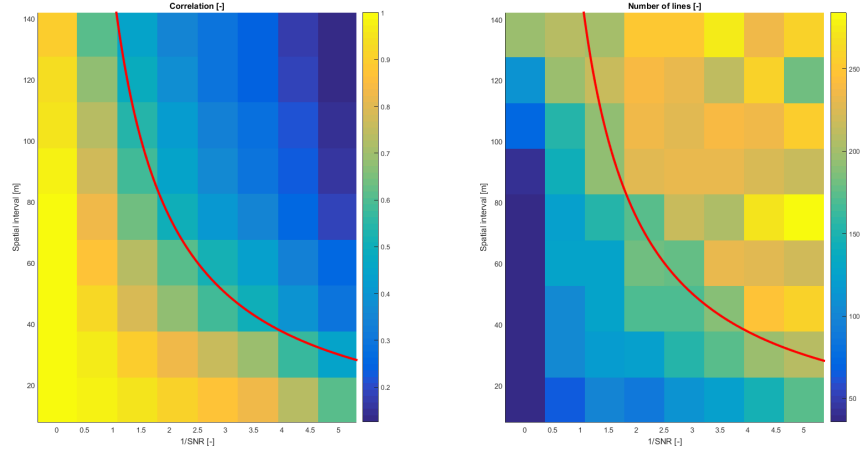
Figure 15: Left: matrix of correlation coefficients, where the colour ranges from 0, blue, to 1, yellow. Right: matrix of number of lines, colour ranges from 0, blue, to 290, yellow. From bottom to top the spatial interval is increased, from left to right the SNR decreases for both plots. The super imposed thick red line is the line where $SI/SNR = 75$, thus left of this line is considered good quality.
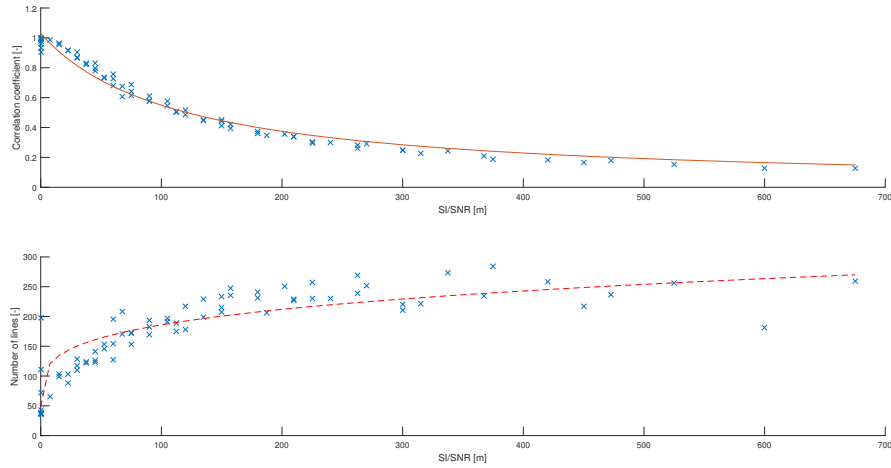

Figure 16: Top: correlation as a function of spatial interval divided by SNR. Bottom: number of lines as found by the canny method. as a function of spatial interval divided by SNR.
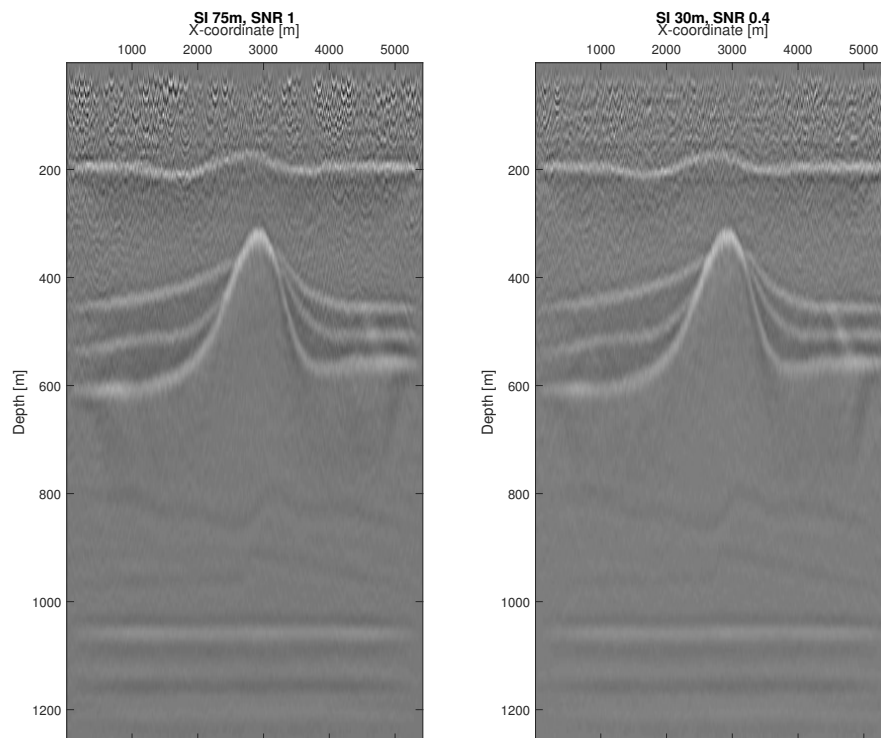
Figure 17: Both plots with $SI/SNR = 75$, the left plot has SI 75m and SNR 1, the right plot has SI 30m and SNR 0.4. In this case the left plot is slightly preferred, even though having the same SI/SNR, since the high SNR makes for better resolved layers below the salt itself, thus what has been considered reservoir in this example, is better visible.

7 Recommendations for future research

Further research should first look into parameters which are currently used in industry to define image quality. Which parameters are used, and what are their threshold values? This will be a literature based study, after which a programming exercise can be undertaken to model these parameters, verify their thresholds and possibly find new parameters and/or thresholds.

The two methods used here should be verified against more models, and also extended to 3D. Especially the number of lines parameter needs a better fitted function, which also adheres to the physics behind it.

References

[1] Canny, John, *A Computational Approach to Edge Detection* IEEE Transactions on Pattern Analysis and Machine Intelligence, Vol. PAMI-8, No. 6, 1986, pp. 679-698.

[2] Campman, X., Behn, P., Faber, K., *Sensor density or sensor sensitivity?* The leading edge, July 2016p. 578-585

[3] Dean, T, *Land seismic: the 'quiet' revolution* Preview **157**, 38-41

[4] Fokkema, J.T., Van den Berg, P.M., *Seismic applications of acoustical reciprocity* Elsevier Science Publ. Co., Inc., 1993

[5] Hagelund, R., Stewart A. Levin, eds. *SEG-Y r2.0: SEG-Y revision 2.0 Data Exchange format* Society of Exploration Geophysicists, Tulsa, OK, 2017

[6] Schulte, B. W., Manthei, D., *Chasing Density – An Introduction to Seismic Acquisition, Processing, and Interpretation Methods Leading to Quantitative Interpretation* Secorder, vol. 39, No. 08, CSEG, 2014

[7] Tellier, N., Lainé, J., *Understanding MEMS-based digital seismic sensors* First Break, vol. 35, is. 1, 2017

[8] Vermeer, G. J. O., *Creating image gathers in the absence of proper common-offest gathers* Exploration Geophysics **29** 636-642, 1998

[9] Vermeer G. J. O., *3-D Seismic Survey Design* Society of Exploration Geophysicists, 2002

[10] Wu Y., Wang B. and Yin W., Li G., *High density wide line acquisition technology and its application at Nyima basin, Tibet, China*, SEG International Exposition and 87th Annual Meeting, 2017

[11] Schlumberger Oilfield Glossary, for all geological and geophysical terminology related to the petroleum sector: http://www.glossary.oilfield.slb.com/

Finally, I would like to thank Joost for the discussions on the figures and plots and how to visually represent them.

9   Appendix

Table 4: Article names and authors belonging to table3 . All presented on the 77th, 78th, or 79th EAGE conferences unless stated otherwise

Study name	Citation
Th A3 09	Al-Mutairi, A. et al., A Case Study of Monitoring Steam Flood Projects in Thin Vertically Stacked Reservoirs Using 3DVSP Technology, 2017
Th A3 12	Humphries, M., Hard Rock VSP - The Case of the Missing P-wave, 2017
Th P6 04	Zhang, F.J., Cross-correlation or Autocorrelation - A Passive Seismic Interferometry Example from Ketzin CO2 Geological Storage Site, 2017
Tu A2 17a,b	Saleh, A., et al., A Step Change in Seismic Imaging Quality in Western Desert of Egypt - An Acquisition Case Study,2017
Tu B3 08	Jamali, J., et al., Reverse Time Migration with Coherent Stacking - A Successful Application on Land Data with Rough Topography, 2017
We A3 07	Sedova, A., et al., High-resolution Land Full Waveform Inversion - A Case Study on a Data Set from the Sultanate of Oman, 2017
We A3 08	Consolvo, B.P., et al., FWI with Scaled-Sobolev Preconditioning Applied to Short- Offset Vibroseis Field Data,2017
We B3 09a,b,c,d	Michou,. L., et al., Survey Design Comparison Regarding Seismic Reservoir Characterization Objectives - A Case Study from South Tunisia, 2017
Th SRS3 07	Naumann, S., et al., Enhanced Subsurface Illumination of Shallow Bright Spots with Separated Wavefield Imaging, 2016
. . .	Seeni, S., et al., Enhanced Subsurface Illumination of Shallow Bright Spots with Separated Wavefield Imaging, IPTC 13616, 2009 *Not from EAGE conference*
We P5 12a,b	Panea, I., Mocanu, V., Eastern Pannonian Basin Analysis of Geothermal Behaviour by Integrated Geophysical Information, 2016
Th N114 06	Ourabah, A., et al., Impact of Acquisition Geometry on AVO/AVOA Attributes Quality - A Decimation Study Onshore Jordan, 2015
Th P7 02	Zhang, B.Q., et al., Wide-azimuth, Broadband, and High-density 3D Seismic Survey in Eastern Edge of the Pre- Caspian Basin, 2015
Th P7 06	Neklyudov, D., et al., Enhancing 3D Broadband Land Seismic Data with Smart Super Groups for Processing and FWI, 2015
Th P7 08	El-Emam, A.H., et al., Quantitative Analysis of Point Receiver 3D Seismic for Optimum and Cost Effective Survey Design, Case Study, 2015
Tu P3 02	Gong, L., et al., TTI Anisotropic PSDM in a Permafrost Region - A Case Study of Point Thomson, North Slope, Alaska, 2015